Energy Engineering

Tech Science Press

DOI: 10.32604/ee.2024.057720

ARTICLE

Recent Advancements in the Optimization Capacity Configuration and Coordination Operation Strategy of Wind-Solar Hybrid Storage System

Hongliang Hao[1], Caifeng Wen[2,3], Feifei Xue[2,*], Hao Qiu[1], Ning Yang[2], Yuwen Zhang[1], Chaoyu Wang[1] and Edwin E. Nyakilla[1]

[1]Department of New Energy Storage, Peking University Ordos Research Institute of Energy, Ordos, 017010, China

[2]School of Energy and Power Engineering, Inner Mongolia University of Technology, Hohhot, 010080, China

[3]Key Laboratory of Wind Energy and Solar Energy Utilization Technology, Inner Mongolia University of Technology, Hohhot, 010051, China

[*]Corresponding Author: Feifei Xue. Email: 20231800271@imut.edu.cn

Received: 26 August 2024 Accepted: 28 October 2024 Published: 27 December 2024

ABSTRACT

Present of wind power is sporadically and cannot be utilized as the only fundamental load of energy sources. This paper proposes a wind-solar hybrid energy storage system (HESS) to ensure a stable supply grid for a longer period. A multi-objective genetic algorithm (MOGA) and state of charge (SOC) region division for the batteries are introduced to solve the objective function and configuration of the system capacity, respectively. MATLAB/Simulink was used for simulation test. The optimization results show that for a 0.5 MW wind power and 0.5 MW photovoltaic system, with a combination of a 300 Ah lithium battery, a 200 Ah lead-acid battery, and a water storage tank, the proposed strategy reduces the system construction cost by approximately 18,000 yuan. Additionally, the cycle count of the electrochemical energy storage system increases from 4515 to 4660, while the depth of discharge decreases from 55.37% to 53.65%, achieving shallow charging and discharging, thereby extending battery life and reducing grid voltage fluctuations significantly. The proposed strategy is a guide for stabilizing the grid connection of wind and solar power generation, capability allocation, and energy management of energy conservation systems.

KEYWORDS

Electric-thermal hybrid storage; modal decomposition; multi-objective genetic algorithm; capacity optimization allocation; operation strategy

Nomenclature

δ	Power fluctuation in time interval t
$P_{max}(t)$ & $P_{min}(t)$	Maximum output power and minimum power in time interval t
$P_{ave}(t)$	Average power in time interval t
$P_{origin,n}$	Raw signal power
$P_{grid,n}$	Grid-connected power
$P_{hess,n}$	Hybrid energy storage power
P_{high} & P_{low}	High-frequency component and crossover component after IMF reconstruction

$P_{2f(p)}$	The power value in the p-order component is reconstructed at low frequency
$P_{\lim it}$	Fluctuation limit
SOC_{secmax} & SOC_{secmin}	The upper and lower limits of the normal working area of energy storage
$SOC_{\min stop}$ & $SOC_{\max stop}$	Storage system SOC upper and lower warning limits
$SOC_{\max}$ & $SOC_{\min}$	Upper and lower limits of emergency area for storage
C	Combined energy storage cost
C_{Bat}^{Li} & C_{Bat}^{LA} & C_{Heat}	Lithium ion, lead-acid battery energy storage cost, thermal energy storage cost
$C_{Bat,Li}^{inv}$ & $C_{Bat,LA}^{inv}$ & C_{Heat}^{inv}	Lithium battery, lead-acid battery energy storage investment cost, heat storage investment cost
C_{BLi1}^{inv} & C_{BLA1}^{inv}	Unit capacity investment cost of lithium battery and lead-acid battery
$C_{\tan k1}^{inv}$	Unit capacity investment cost of heat storage tank
C_{boiler}^{inv}	Electric boiler heater investment cost
$C_{Bat,Li}^{oper}$ & $C_{Bat,LA}^{oper}$ & C_{Heat}^{oper}	Lithium battery, lead-acid battery energy storage and hot storage operation and maintenance cost
C_{comp}	Comprehensive power compensation cost
$C_{comp+}n(t)$ & $C_{COMP-}n(t)$	Positive undercompensated power and negative undercompensated power at time n
n_1 & n_2 & n_3	Number of lithium-ion batteries, lead-acid batteries, and heat storage tanks
r_1 & r_2 & r_3	Depreciation rate of lithium ion, lead-acid batteries and heat storage tanks and electric boiler heaters
$C_{BLi,rate}^{inv}$ & $C_{BLA,rate}^{inv}$	Lithium battery, lead-acid battery unit capacity rated investment cost
$C_{\tan k}^{inv}$	Rated investment cost per unit capacity of heat storage tank
$C_{BLi,Nd}$ & $C_{BLA,Nd}$	Preferential cost per unit capacity of lithium-ion and lead-acid batteries
$C_{\tan k,Nd}$	Preferential cost per unit capacity of heat storage tank
c_1 & c_2 & c_3	Cost preference factor
η	Power cost factor of electric boiler heater
α & ε & μ	The ratio of the operating and maintenance cost of lithium batteries, lead-acid batteries and heat storage systems to the investment cost
N_c	Battery equivalent cycle life
Dod	Depth of discharge
β (Dod, i)	Equivalent charge-discharge cycle coefficient of a battery
O & M	Operation and maintenance

1 Introduction

Renewable energy from wind and photovoltaic power generation are intermittency and unpredictable energy sources, that seriously affect the normal function of the power system [1–3]. The fluctuations in energy sources bring serious challenges to the power quality and stability of the grid network [4–7]. Coupling electrical grid systems with different aspects of power production can increase power production flexibility and plant operation [8–11]. The use of an energy storage system of charging and discharging can smoothly encounter the output power fluctuations and flexibly adjust the power imbalance situation, which not only affects the supply, demand, and balance of the power system but also solves the intermittency and volatility of wind power and photovoltaic power generation [12,13]. This results in the enhancement of country revenue through constant power supply

in the industry and production sectors [14–17]. Based on this, it is vital to introduce a hybrid wind-solar energy storage system to reduce the power fluctuation impact on the power grid and to improve the stability of the power grid.

Recently, the use of renewable energy has drawn much attention around the world [18–21]. Solar energy technology, as a crucial origin of renewable energy, has long-term merits, improves sustainability, and encounters pollution [22–25]. Despite, providing flexible power, it faces challenges due to the occasional energy source [26–29] On the other hand, Concentrated Solar Power (CSP) has drawn much attention in recent years, due to its flexibility and capability to be incorporated with other sources of energy like thermal energy [30–33]. Wen et al. [26] aimed at the problems of large loss and low efficiency of wind power generation system, multi-field coupling method was adopted to conduct multidimensional analysis of electromagnetic field and temperature field in wind power generation system, and the system loss region was accurately obtained, and the wind power generation efficiency was improved by optimizing the composition structure of wind power generation system. Wen et al. [27] proposed a wind power + energy storage model to explore the influence of different energy storage modes on various power quality indicators in wind power generation, and Ansys software was used to simulate and explore the inside of the wind power generation system. Liu et al. [28] proposed a solar power plant with multiple combinations, including photovoltaic power station, thermal storage system, Concentrated Solar Power (CSP) and other equipments, and takes standardized energy cost and power failure probability as evaluation criteria to obtain the best component coordination and capacity configuration through multi-objective optimization. The results show that the proposed system can effectively reduce power generation costs and improve power generation reliability. Kandi et al. [29] proposed a new type of solar power generation and energy storage power station, which is mainly composed of Thermal Electric Generator (TEG) and Phase Change Material (PCM), which can effectively improve energy storage efficiency. At present, there are few studies on PCM integrating TEG, and this field has great research prospects.

Moreover, wind energy commonly contains the most negligible effect on climate change compared to other sources of energy like fossil fuels [34–37] A wind turbine is used to produce electricity [38]. On the contrary, it faces challenges such as weather variation and high load requirements in some areas [39–42]. The main challenge of using wind and solar energy is their constant weather dependence [43,44] Consequently, a hybrid renewable energy system is necessary to ensure a constant supply of energy.

Hybrid wind and solar energy can be converged to encounter the fluctuation of high energy demand through different forms of energy storage, so as to ensure the stability of the power grid. Moreover, References [45–47] proposed an Intelligent Adaptive Control (IAC) architecture to address the impact of renewable energy on microgrids due to various meteorological factors. The architecture was designed by combining Artificial Neural Network-Proportional Integral (ANN-PI) and regulated voltage by adjusting the inverter secondary network. The experimental findings proved that IAC architecture could effectively reduce microgrid fluctuations. Likewise, Mahesh et al. [48] proposed a genetic algorithms approach to optimize hybrid solar photovoltaic-wind-battery systems and found that genetic algorithms minimized cost while maintaining power stability. Multi-objective genetic algorithm has a strong global search ability and high processing complexity, which is suitable for complex constraints and targets in the allocation of scenery capacity. Moreover, the population nature of genetic algorithm enables it to process multiple solutions in parallel and has high efficiency. Therefore, this paper chooses to use multi-objective genetic algorithm to solve the objective function. Based on this, it is vital to enhance the power grid through a hybrid energy system.

This paper presents a wind-solar hybrid energy storage system combining electricity and heat through the optimization of efficiency system of electric-thermal combined energy storage. Secondly, it investigates the primary allocation of wind and solar power through empirical modal decomposition to obtain the grid-connected power to avoid the phenomenon of insufficient or excessive grid-connected power suppression through HESS capacity configuration [49,50]. This work will help the global energy sector to mitigate the effect of intermittent energy challenges and enhance operation strategy through power volatility, economy, and power quality control.

2 Model of Wind-Photovoltaic and Storage System

In this work, a wind-solar hybrid model was developed to analyze the energy potential of a coupled energy system. The structure of the wind-solar hybrid energy storage system is shown in Fig. 1. It mainly consists of a power generation system, a hybrid energy storage system, a load, and a process switching system utilized for monitoring wind and solar power production systems and different energy storage scenarios.

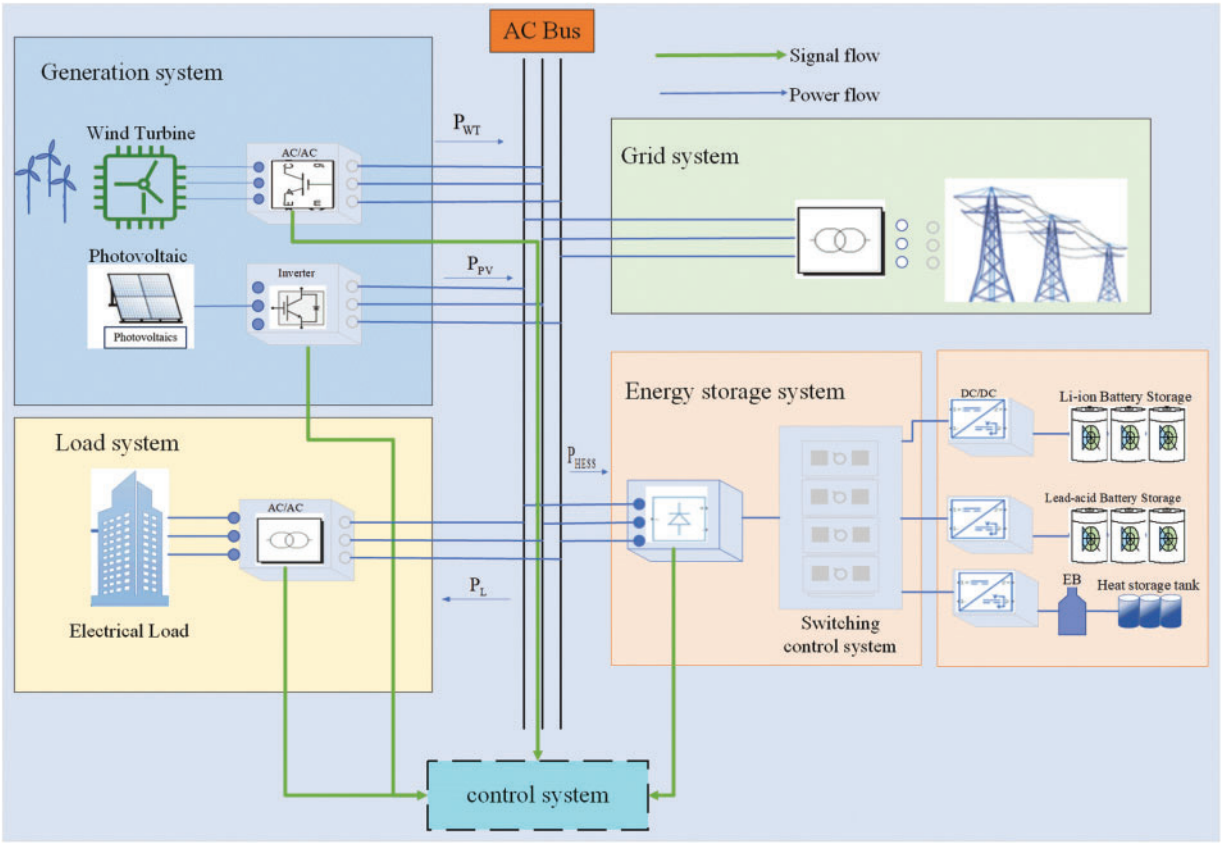

Figure 1: Diagram of hybrid energy storage systems for wind power generation

Wind farms and photovoltaic power plants were used to generate power for the grid and energy storage and consumption depending on the power utility. If the power volatility is large it will affect the power quality and reliable operation. In utilizing the wind and solar complementary system, the first part is the power generation system, load system, control system, grid system, and energy storage

system are all smoothed out. Hybrid energy storage implemented in this work consists of battery and thermal storage. The complementary power of wind and solar output meets the power merger and acquisition of grid-connected fluctuations through power decomposition and carries out energy storage if it does not meet the requirements and further rational distribution of electric heating energy storage in the process of energy storage and release.

2.1 Fluctuating Characteristics of Wind and Photovoltaic Generation

Considering the actual output energy of the system and the degree of operational fluctuation, the power fluctuation rate is defined as the evaluation index, indicated in Eq. (1) below:

$$\delta = \frac{P_{\mathrm{MAX}}(t) - P_{\mathrm{MIN}}(t)}{P_{\mathrm{ave}}(t)} \times 100\% \tag{1}$$

where δ is the power fluctuation rate and t is time interval, $P_{MAX}(t)$ represents maximum, $P_{MIN}(t)$ represent minimum and $P_{ave}(t)$ represents the average power in time interval, respectively.

2.2 Power Allocation Strategy

In power power distribution, the basic idea is to divide the power by high and low frequency. The normalized power signal is obtained by the ratio of the original power signal to the grid-connected power, and the normalized power signal is decomposed into several fixed mode functions (IMFs), which are combined with the fluctuation limit of wind power grid-connected. Each order IMF is reconstructed into a high-frequency component and a low-frequency component by Eqs. (2) and (3), and each IMF represents a frequency component in the original signal. The constraint of wind power fluctuation limit is shown in Eq. (4).

$$P_{\mathrm{low}} = c_{2f(i)} = \sum_{i=m+1}^{k} \mathrm{IMF}i + \mathrm{res} \tag{2}$$

$$P_{\mathrm{high}} = f_{2c(i)} = \sum_{i=1}^{m} \mathrm{IMF}i \tag{3}$$

$$\max P_{c2f(p)} - \min P_{c2f(p)} \leq P_{\lim it} \tag{4}$$

where $P_{c2f(p)}$ is the power value within the pth-order component of the low-frequency reconstruction in the specified time; $P_{\lim it}$ is the fluctuation volume limit. K-means clustering is carried out for the wind-solar power output, modal decomposition is carried out for grid-connection power, and energy storage according to grid-connected limits. The specific power allocation process is shown in Fig. 2.

2.3 Electric-Thermal Hybrid Energy Storage Operation Strategy

In the process of an electric-thermal hybrid energy storage operation, the mode in each area is formulated by delineating different working areas of the energy storage system, as shown in Table 1. Where SOC_{secmax} and SOC_{secmin} represent the upper and lower limits of the normal working area of the energy storage, and also the opening threshold of the heat storage. Likewise, $SOC_{\max stop}$ and $SOC_{\min stop}$ represent the upper and lower alarm limits of the SOC power storage, and $SOC_{\max}$, $SOC_{\min}$ represent the upper and lower limits of the emergency area of the power storage.

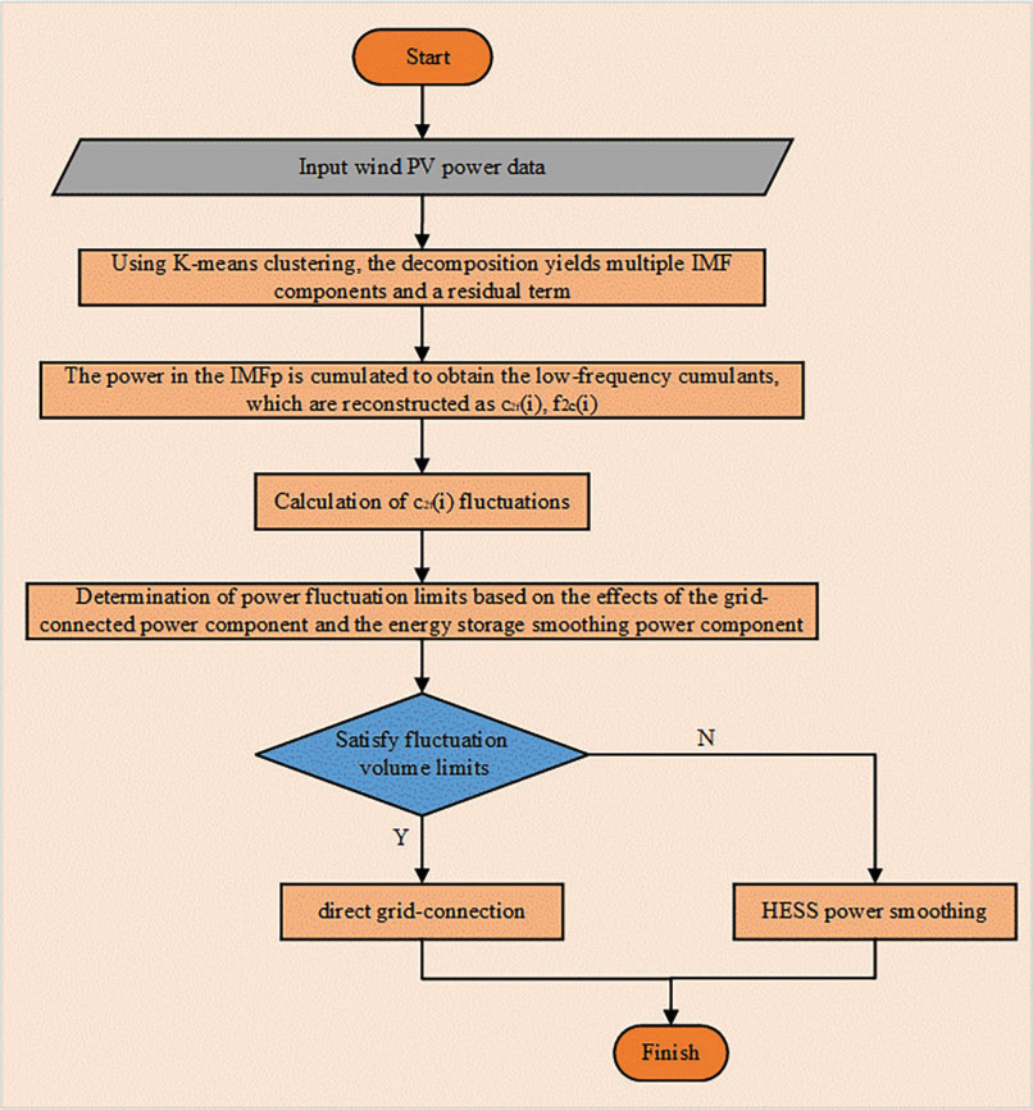

Figure 2: Flow chart of wind PV power allocation strategy

Table 1: Division of the HESS workspace

SOC range	Workspace
$SOC_{\max} \leq SOC < 1$	Energy storage overcharge contingency area
$SOC_{\max stop} \leq SOC \leq SOC_{\max}$	Electric energy storage overcharge zone
$SOC_{secmax} \leq SOC \leq SOC_{\max stop}$	Energy storage overcharge warning zone
$SOC_{secmax} \leq SOC < 1\ S_{\min} \leq S < S_{\max}$	Thermal energy storage thermal operation area
$SOC_{secmin} \leq SOC \leq SOC_{secmax}$	Normal working area of electrical energy storage
$0 < SOC \leq SOC_{secmin}\ S_{\min} < S \leq S_{\max}$	Thermal storage heat release operation zone

(Continued)

Table 1 (continued)

SOC range	Workspace
$SOC_{\min stop} \leq SOC \leq SOC_{secmin}$	Electric storage capacity over-discharge warning area
$SOC_{\min} < SOC \leq SOC_{\min stop}$	Electric storage over-discharge zone
$0 < SOC \leq SOC_{\min}$	Electrical storage over discharge emergency area

Through the SOC seven-region design, the SOC with electrochemical energy storage provides enough power and capacity space, better shallow charging and discharging, to avoid excessive use of electric energy storage, and smooth fluctuations. The energy operation strategy is shown in Table 1. During charging, when SOC_{secmax} is reached and the heat storage is within a reasonable range, the heat storage is turned on. When SOC reaches $SOC_{\max stop}$, the charging is stopped to avoid current sudden change and overcharging of the battery. $SOC_{\max stop} \sim SOC_{\max}$ is reserved as the overcharge buffer area. When the heat storage reaches the maximum, the heat storage is closed. On the contrary, the discharge process is similar. The specific process is shown in Fig. 3 below.

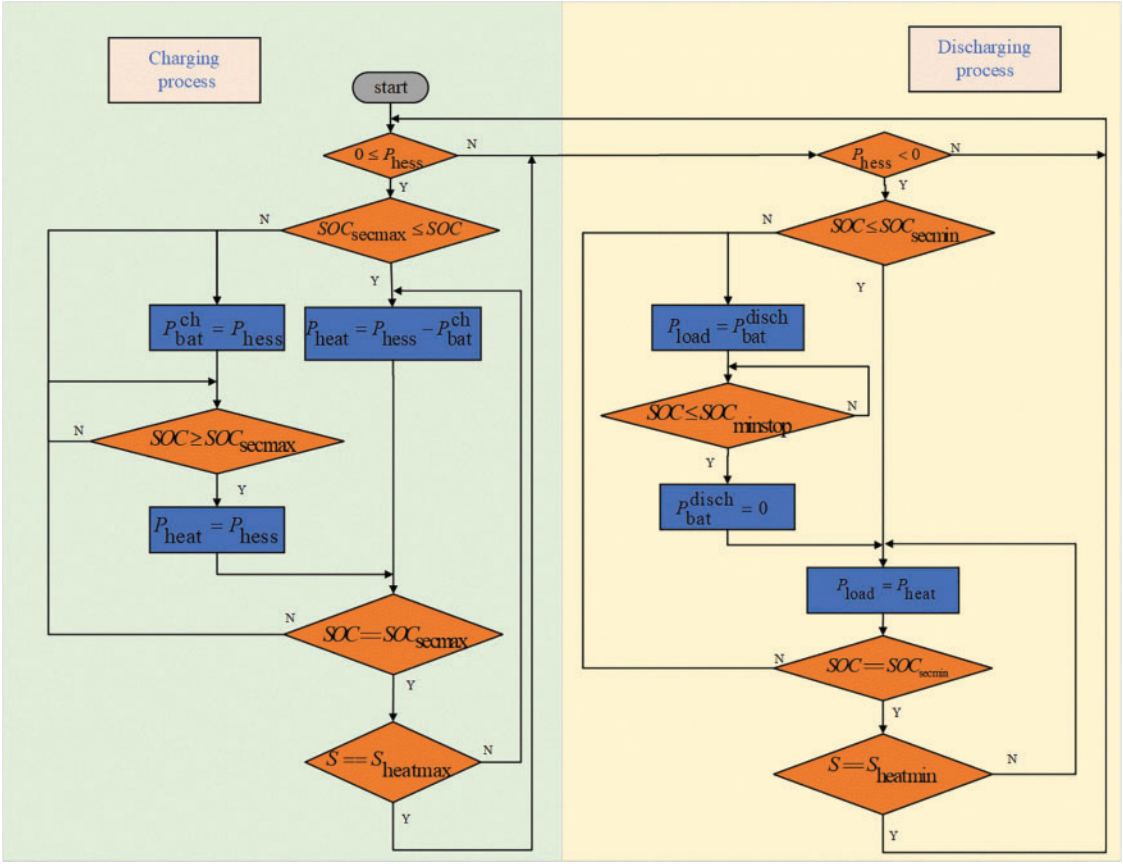

Figure 3: Flow chart of energy management strategy for electric and thermal energy storage

3 Hybrid Energy Storage Capacity Optimization Model

3.1 Objective Function

For several combined objective optimization allocation problem for a wind-source hybrid energy storage system, the lowest comprehensive cost and the longest cycle life are set as the optimization objectives function under the premises to ensure a stable and reliable operation system. For hybrid energy storage capacity, with the lowest comprehensive cost and the longest cycle life as optimization objectives, the multi-objective genetic algorithm is used to optimize the electric heating energy storage configuration. The objective function is expressed as indicated in Eq. (5), as previously explained by

$$\min C = C_{\text{Bat}}^{\text{Li}} + C_{\text{Bat}}^{\text{LA}} + C_{\text{Heat}} + C_{\text{comp}} \tag{5}$$

where C is the comprehensive energy storage cost, C_{Bat}^{Li} is the lithium-ion battery energy storage cost, C_{Bat}^{LA} is the lead-acid battery energy storage cost, C_{Heat} is the thermal energy storage investment operating cost, and C_{comp} base power compensation cost, where C_{Bat}^{Li}, and C_{Heat} are expressed as Eq. (6).

$$\begin{cases} C_{\text{Bat}}^{\text{Li}} = C_{\text{Bat,Li}}^{\text{inv}} + C_{\text{Bat,Li}}^{\text{oper}} \\ C_{\text{Bat}}^{\text{LA}} = C_{\text{Bat,LA}}^{\text{inv}} + C_{\text{Bat,LA}}^{\text{oper}} \\ C_{\text{Heat}} = C_{\text{Heat}}^{\text{inv}} + C_{\text{Heat}}^{\text{oper}} \end{cases} \tag{6}$$

where $C_{Bat,Li}^{inv}$ and $C_{Bat,LA}^{inv}$ are the investment costs of lithium and lead-acid battery storage, $C_{Bat,Li}^{oper}$ and $C_{Bat,LA}^{oper}$ are the operation and maintenance costs of lithium and lead-acid battery storage, C_{Heat}^{inv} and C_{Heat}^{oper} are the investment costs and operation and maintenance costs of thermal storage respectively Eqs. (7) and (8).

(1) Investment costs

The investment cost expression is as follows:

$$\begin{cases} C_{\text{Bat,Li}}^{\text{inv}} = n_1 C_{\text{BLi1}}^{\text{inv}} (1 - r_1) \\ C_{\text{Bat,LA}}^{\text{inv}} = n_2 C_{\text{BLA1}}^{\text{inv}} (1 - r_2) \\ C_{\text{Heat}}^{\text{inv}} = \left(n_3 \times C_{\text{tank1}}^{\text{inv}} + C_{\text{boiler}}^{\text{inv}}\right) (1 - r_3) \end{cases} \tag{7}$$

$$\begin{cases} C_{\text{BLi1}}^{\text{inv}} = C_{\text{BLi,rate}}^{\text{inv}} - \left(c_{\text{BLi,Nd}} \times n_1\right) + c_1 \\ C_{\text{BLA1}}^{\text{inv}} = C_{\text{BLA,rate}}^{\text{inv}} - \left(c_{\text{BLA,Nd}} \times n_2\right) + c_2 \\ C_{\text{tank1}}^{\text{inv}} = C_{\text{tank,rate}}^{\text{inv}} - \left(c_{\text{tank,Nd}} \times n_3\right) + c_3 \\ C_{\text{boiler}}^{\text{inv}} = C_{\text{boiler1}}^{\text{inv}} \times \eta \end{cases} \tag{8}$$

The investment cost is calculated by the product of the unit capacity investment cost, capacity, and depreciation rate, where the unit capacity investment cost takes into account the actual market preference and adjusts the unit capacity investment cost. Where C_{BLi1}^{inv} and C_{BLA1}^{inv} are the unit capacity investment costs of lithium-ion and lead-acid batteries respectively, n_1 and n_2 denote the number of lithium-ion batteries and lead-acid batteries, respectively, and $C_{\tan k1}^{inv}$ is the unit capacity investment cost of the heat storage tank, C_{boiler}^{inv} is the investment cost of the electric boiler heater, and n_3 is the number of heat storage tanks. r_1, r_2 and r_3 are the depreciation rates for lithium-ion, lead-acid batteries, thermal storage tanks, and electric boiler heaters, respectively. $C_{Bli,rate}^{inv}$, $C_{BLA,rate}^{inv}$ and $C_{\tan k,rate}^{inv}$ are the nominal investment costs per unit capacity of lithium-ion batteries, lead-acid batteries, and thermal storage tanks, respectively. $c_{Bli,Nd}$, $c_{BLA,Nd}$ and $c_{\tan k,Nd}$ are the preferential costs per unit capacity of lithium-ion,

lead-acid batteries, and heat storage tanks, respectively. c_1, c_2 and c_3 are the cost preference factors. η is the power cost factor of the electric boiler heater.

(2) Operation and maintenance costs

Operation and maintenance can be simplified by estimating it as a percentage of the investment cost expressed in Eq. (9).

$$\begin{cases} C_{\text{Bat,Li}}^{\text{oper}} = \alpha C_{\text{Bat,Li}}^{\text{inv}} \\ C_{\text{Bat,LA}}^{\text{oper}} = \varepsilon C_{\text{Bat,LA}}^{\text{inv}} \\ C_{\text{Heat}}^{\text{oper}} = \mu C_{\text{Heat}}^{\text{inv}} \end{cases} \tag{9}$$

where α, ε and μ are the coefficients of the ratio of the operation and maintenance cost of the electrochemical energy storage system and heat storage system to the investment cost, which are positively correlated with the investment.

(3) Compensation costs for wind energy output fluctuations

When the power of wind fluctuates greatly, the high-frequency fluctuation component of wind power output that exceeds the upper limit of the power of the energy storage system needs is supplemented by dispatching other resources, which increases the compensation cost, as measured in Eq. (10).

$$C_{\text{comp}} = \sum_{t=1}^{N} c_{\text{comp}} \left(P_{\text{comp+,n}}(t) - P_{\text{comp-,n}}(t) \right) \tag{10}$$

where c_{comp} is the base power compensation cost coefficient, $P_{\text{comp+,n}}(t)$ and $P_{\text{comp-,n}}(t)$ are the positive under-compensated power and negative under-compensated power at moment n, respectively.

(4) Cycle life model

The life cycle for a device of energy storage mainly consider the effect of battery discharge depth (Dod) on battery life. The relationship between the depth of discharge and cycle life of Li-ion batteries according to [48] is shown in Table 2.

Table 2: Relationship between lithium battery discharge and cycle life

Depth of discharge/%	Cycle life/times	Depth ofdischarge/%	Cycle life/times
10	25,000	60	4167
20	12,500	70	3571
30	8333	80	3125
40	6250	90	2778
50	5000	100	2500

The relationship between depth of discharge and cycle life was fitted using the multiplicative power function approximation Eq. (11).

$$N_{\text{c}} = 249992/\text{Dod} \tag{11}$$

where N_c is the equivalent cycle life of the battery; Dod is the depth of discharge. The equivalent charge/discharge cycle factor of the battery is defined as

$$\beta\,(\mathrm{Dod},i) = N_c\,(\mathrm{Dod},1)\,/N_c\,(\mathrm{Dod},i) \tag{12}$$

where Dod, i is the depth of the battery when the number of discharges is I, N_c (DOd, i) is the cycle of life when the depth of discharge is Dod, i where the value β is usually set as the cycle life when the depth of discharge is 100%. It is usually set as the cycle life at 100% discharge depth, and β range of 0–1. Battery discharge depth and cycle life are shown in Fig. 4.

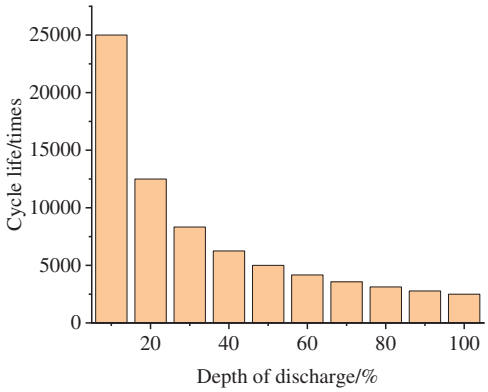

Figure 4: Diagram of the relationship between battery discharge depth and cycle life

3.2 Model Constraints

The charge and discharge power constraints for energy storage devices in this work are stipulated below, where the energy storage device charging and discharging power constraint can be expressed as in Eq. (13).

$$P_{\mathrm{x}} = P_{\mathrm{grid}} + P_{\mathrm{WT}} + P_{\mathrm{PV}} - P_{\mathrm{load}} \tag{13}$$

where at $P_{\mathrm{x}} > 0$ denotes charging of the energy storage system and denotes $P_{\mathrm{x}} < 0$ discharging of the energy storage system. The constraints are shown in Eq. (14) below:

$$\begin{cases} 0 < P_{\mathrm{x}}^{\mathrm{ch}} \le P_{\max} \\ P_{\min} \le P_{\mathrm{x}}^{\mathrm{disch}} \end{cases} \tag{14}$$

Electrothermal hybrid energy storage system, both electrochemical and thermal energy storage systems should be charged and discharged within the appropriate range of SOC constraints as in Eq. (15).

$$\begin{cases} S_{\mathrm{BLi,minstop}} \le S_{\mathrm{BLi}}\,(t) \le S_{\mathrm{BLi,maxstop}} \\ S_{\mathrm{BLA,minstop}} \le S_{\mathrm{BLA}}\,(t) \le S_{\mathrm{BLA,maxstop}} \\ S_{\mathrm{Heat,minstop}} \le S_{\mathrm{Heat}}\,(t) \le S_{\mathrm{Heat,maxstop}} \end{cases} \tag{15}$$

where in the formula above, $S_{BLi,\max stop}$ and $S_{BLi,\min stop}$ are the upper and lower limits of SOC for lithium batteries, $S_{BLA,\max stop}$ and $S_{BLA,\min stop}$ are the upper and lower limits of SOC for lead-acid batteries, and $S_{Heat,\max}$, and $S_{Heat,\min}$ are the upper and lower limits of SOC for heat storage tanks. The specific optimization flow chart is shown in Fig. 5.

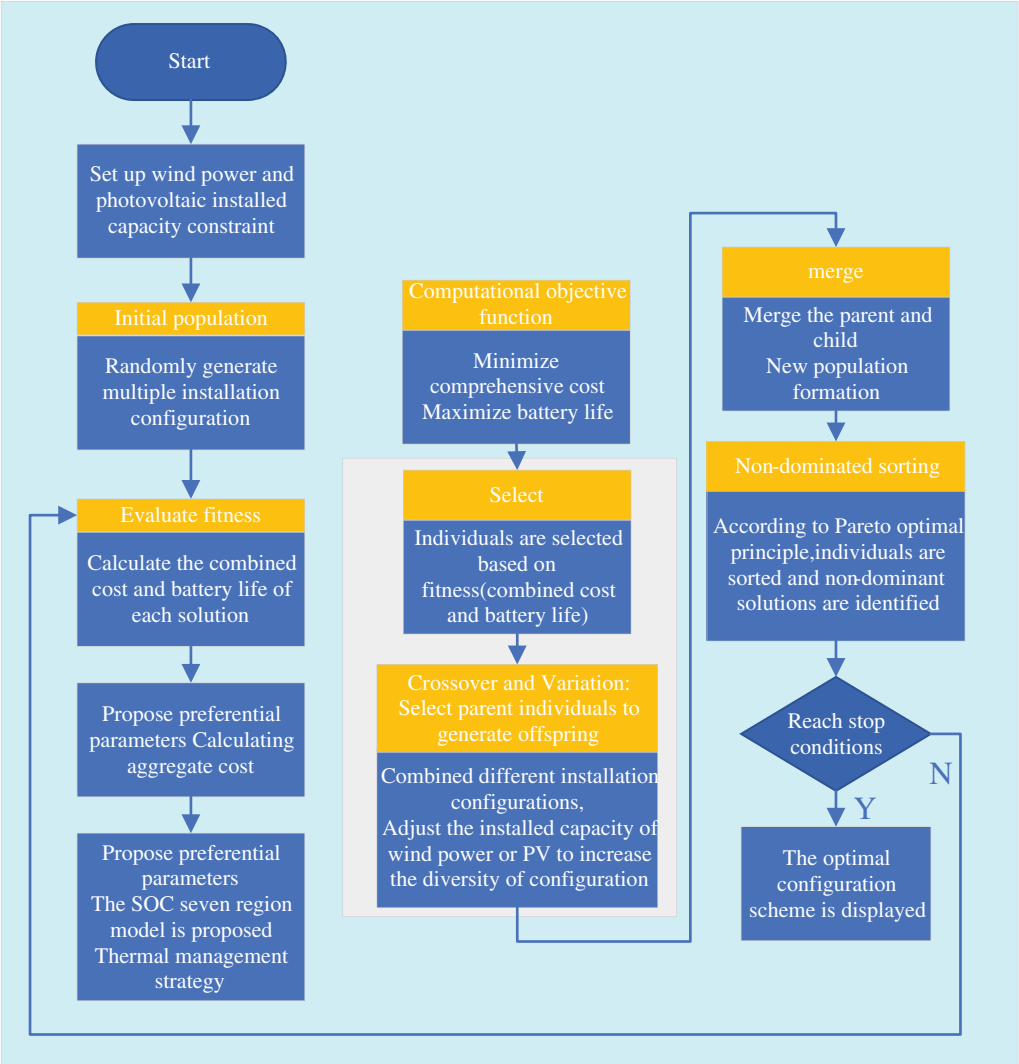

Figure 5: Flow chart of wind-wind capacity configuration optimization algorithm

4 Simulation Analysis

4.1 Analysis of System Operation

Based on MATLAB/Simulink and Real Time Labratory (RT-LAB) semi-physical simulation platform, a wind-source hybrid energy storage system was constructed. Both the wind speed and solar irradiance models are fitted with real-world wind speed and solar irradiance data and are used as inputs to the wind turbine model and the PV model. The rated capacity of the electrochemical energy storage system in the system depends on the installed capacity configuration of the wind power generation system, and the electrochemical energy storage model did not consider the effects of temperature and cycle life. The electric boiler in the thermal storage system model adopts a multi-stage heating mode, and the water supply tank is regarded as an infinite water source. The basic parameters of the system are shown in Table 3.

Table 3: Basic parameters

Parameters	Value	Parameters	Value
Wind speed (m/s)	5–12	Solar irradiance (W/m^2)	500–1150
Wind turbine rated power (MW)	0.5	Rated water supply flow rate of water storage tank (kg/s)	5
PV rated power (MW)	0.5	Total rated power of electric boiler (kW)	500
Rated grid voltage (KV)	400	Rated power of electrical load (kW)	300
Initial SOC for electrochemical energy storage (%)	60	Thermal load rated power (kW)	300

The results of wind and PV power volatility curves are shown in Fig. 6. It can be seen that from a time perspective, the two changes are complementary, thus, the PV power fluctuations with time at the point of wind power volatility are smaller, likewise the wind power fluctuations in the node of the PV fluctuation are also smaller. Moreover, the volatility of wind power and PV after complementary is demonstrated in Fig. 7.

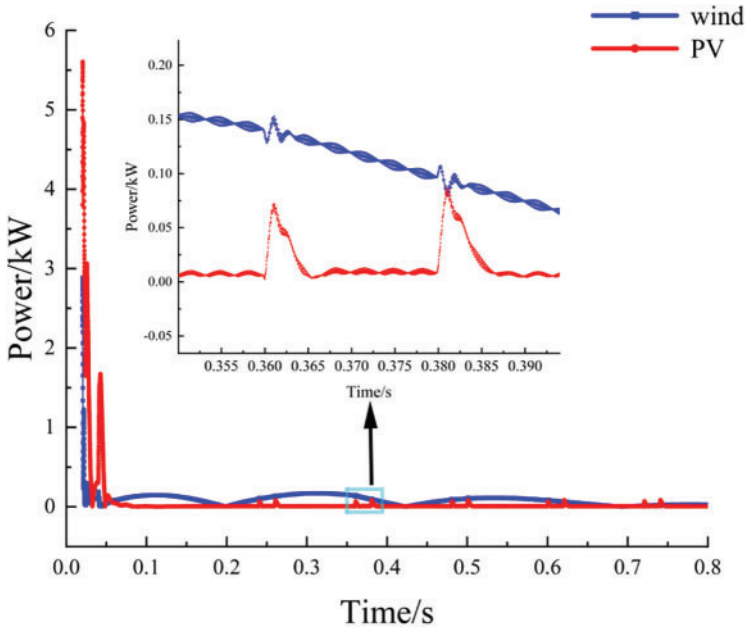

Figure 6: Graph of power fluctuations in wind and photovoltaic power generation

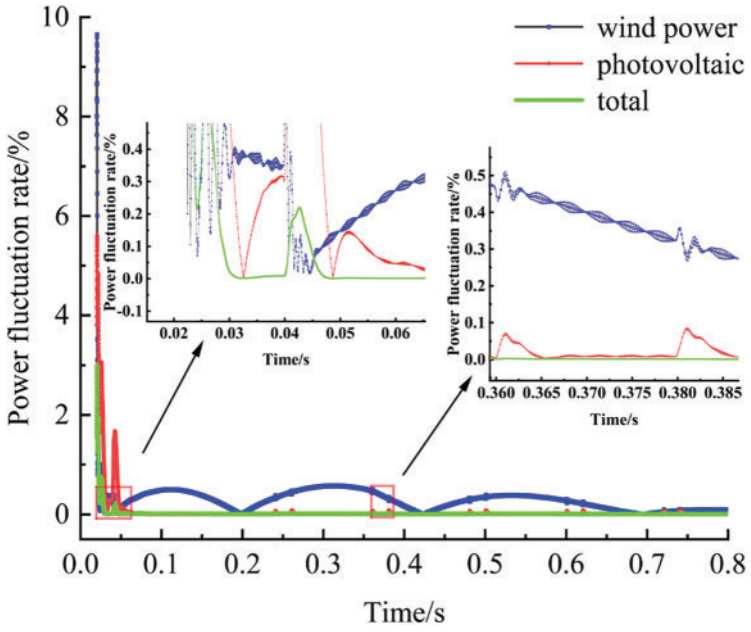

Figure 7: Wind, PV, and total power volatility graphs

It is indicated that the power fluctuation in the wind and photovoltaic hybrid power generation begins at 0.047 and 0.31 s, respectively. This produces the weak wave peak within the fluctuation rate of 0.59, The fluctuation of PV at 0.27 s is 0.09. The variation characteristics of wind energy and PV are not completely lifetime capable of achieving the volatility of the mutual offset.

4.2 Power Distribution

Before power allocation, to avoid the effect of extreme data, the data were clustered. The K-means algorithm was used to cluster the 5 s scenery data to obtain four scenery power-out scenarios. The time and probability corresponding to each scenario are listed below in Table 4. The median cumulative fluctuation is used as an indicator for each scenario, and the selected clustering scenarios are shown in Table 4.

Table 4: Duration and probability of different scenarios

Scenario	Data value	Duration (s)	Probability
1	47,352	2.38	29.55%
2	29,429	1.48	47.54%
3	5684	0.29	5.71%
4	17,136	0.86	17.20%

The results of wind energy clustering are indicated in Figs. 8 and 9, where the cluster findings of four scenarios were 514.58, 347.10, −10.78, and 210.28 at each point, respectively.

Moreover, the grid-connection fluctuation volume limit was determined to obtain the grid-connection component and the hybrid energy storage power component. It was discovered that the lower the fluctuation limit occurred, the smoother the direct grid connection of the component.

Likewise, the higher the fluctuation of the energy storage, the better the grid performance. For the case where there is too small, a limit value leads to frequent charging as well as discharging of the power storage system, which increases the loss. Fig. 10 indicates the direct grid-connected component at a fluctuation limit of 30, 20, and 10. It is observed that when the fluctuation occurs, it is reduced to 10 and the waveform is being distorted. Likewise, Fig. 11 indicates the multiple fluctuation volume constraints, where the low-frequency reconfiguration component is greater than the grid-connected fluctuation limit, specifically at 20 indicating the fluctuation in grid-connection.

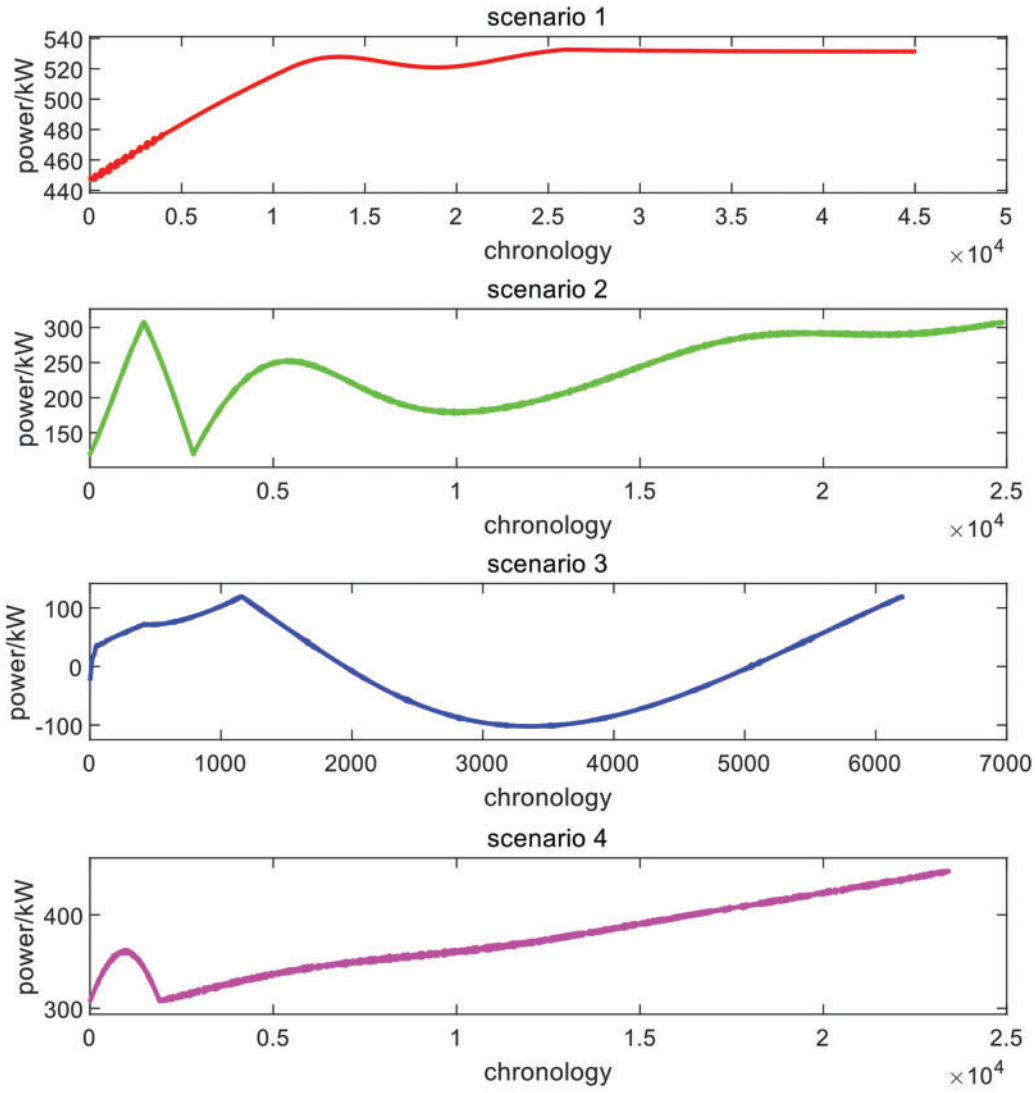

Figure 8: Clustering effect diagram for different scenarios

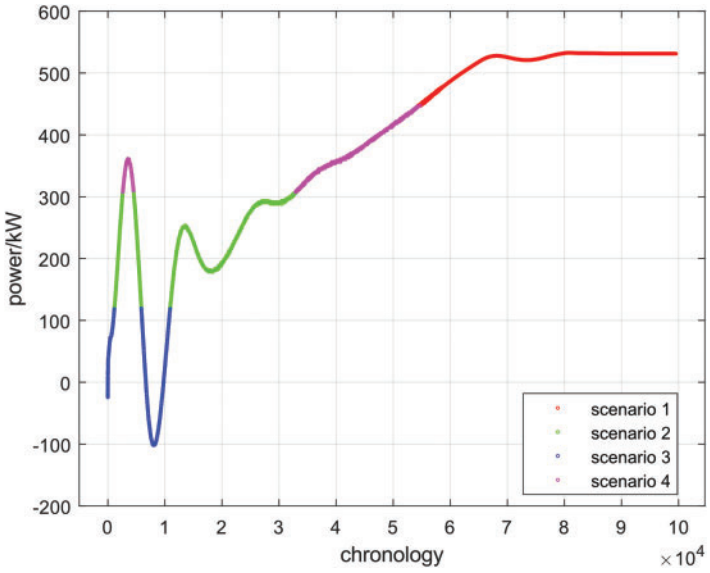

Figure 9: Curves of power output clustering results

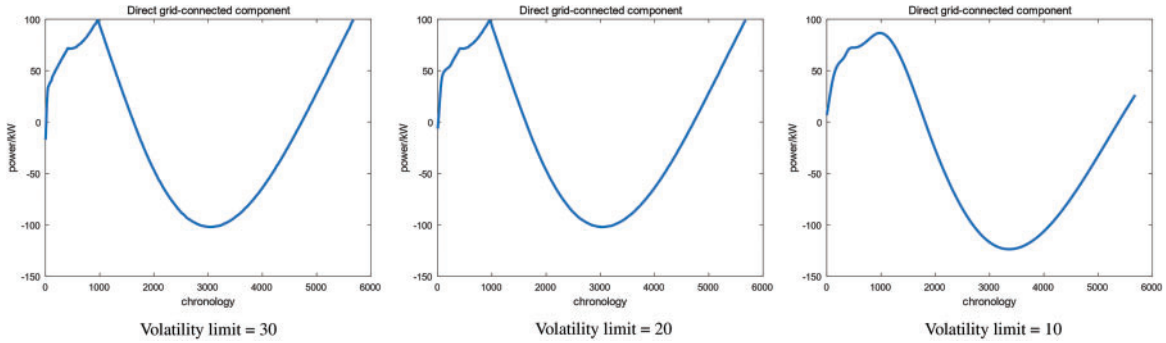

Figure 10: Grid-connected component diagrams for multiple fluctuation-limited quantities

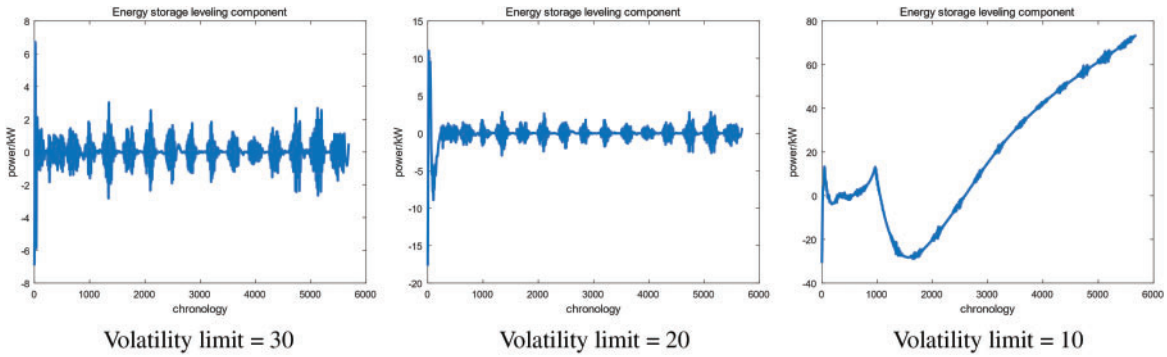

Figure 11: Graph of storage smoothing components under multiple fluctuation volume constraints

The maximum fluctuation of the low-frequency reconfiguration component $c_{2f(4)}$ is close to and not greater than the grid-connected fluctuation limit of 20, as shown in Fig. 12, with the DC grid-connected component of $c_{2f(4)}$ and the hybrid energy storage smoothing component of $c_{2f(5)}$.

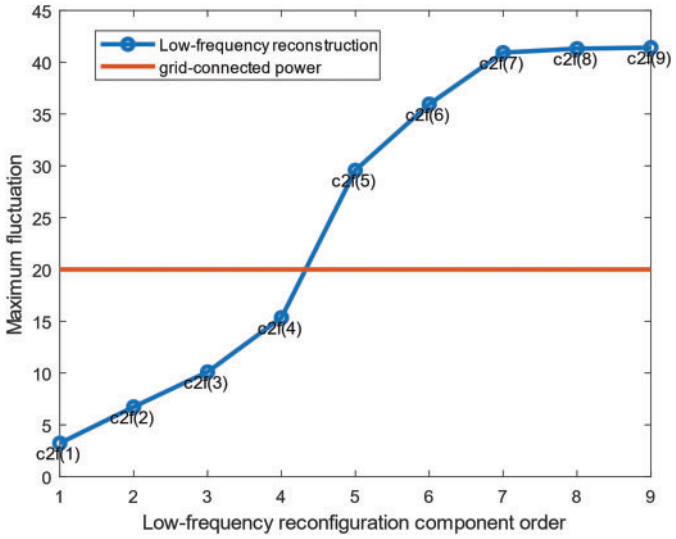

Figure 12: Curves of low-frequency reconstructed component orders

4.3 Configuration Results Analysis

Using the multi-objective optimization genetic algorithm, the hybrid energy storage potential is optimized by the number of lithium batteries, lead-acid batteries, heat storage tanks, storage cost, and the number of electrochemical energy storage cycles as the objective function. The optimized capacity configuration results are shown in Tables 5–7. The comprehensive total cost decreased by 18,006.87 yuan at the total consolidated cost of 24.5%. Lithium battery capacity decreased from the original 400 to 300 Ah, lead-acid battery capacity from the original 300 to 200 Ah. Lithium battery and lead-acid battery capacity decline directly affect the system construction costs, operation, and maintenance costs, while improving the economy of the system. Before optimization, the energy storage cost accounted was 16.7% of the total system cost, and after optimization, it dropped to 12.5%, and the optimization degree was 4.2%. The economic feasibility of the energy storage system configuration was improved through algorithm optimization. The number of electrochemical energy storage in a cycle increased from 4515 to 4660, and the depth of discharge decreased from 55.37% to 53.65%. The main reason for the reduction of all costs is the cost of the battery is higher than the heat storage, and the strategy is utilized to effectively dispatch the heat storage and reduce the cost. Moreover, the depth of discharge was reduced to obtain shallow charging and shallow discharging to improve the battery life.

4.4 Analysis of the Effect of Strategy Optimization

(1) Trend analysis of electrochemical energy storage SOC

Using time charging and discharging cycle data analysis, lithium batteries had a faster decrease in power than lead-acid batteries. Likewise, the rate of charging and discharging was found to be small as shown in Fig. 13.

Table 5: Capacity configuration optimization results

	Lithium battery capacity	Lead-acid battery capacity	Thermal storage tank capacity
Pre-optimization	400	300	100
Post-optimization	300	200	80
Optimal value	100	100	20
Optimization degree	25%	30%	20%

Table 6: Energy storage cost optimization results

	Lithium battery investment cost	Lithium battery O&M costs	Lead battery investment cost	Lead battery O&M costs	Heat storage investment costs	Heat storage O&M costs
Pre-optimization	7608	5072	3291	5059	32,900	18,800
Post-optimization	6066	3033	1971	4204	27,216	12,441.6
Optimal value	1542	2039	1320	855	5684	6358.4
Optimization degree	20.3%	40.2%	40.1%	16.9%	17.3%	33.8%

Table 7: Overall optimization result

	Total consolidated cost	Cycle life/number of cycles
Pre-optimization	684.865	55,407.994
Post-optimization	476.394	73,414.865
Optimal value	208.471	18,006.871
Optimization degree	30.4%	24.5%

Moreover, the chemical characteristics of lead-acid batteries are more easily affected by temperature, charging, and discharging rate during the charging and discharging process, resulting in relatively fast SOC changes. The SOC change rate of Li-ion batteries is lower than that of lead-acid batteries, and Li-ion batteries are more stable and have greater energy density during the charging and discharging process. After optimization, the discharge depth of both batteries is reduced, which helps to extend the service life of the battery and reduce the damage to the battery structure caused by deep discharge. The results show that the proposed strategy achieves shallow charging and shallow discharge, which provides a research direction for considering the service life of electrochemical energy storage.

(2) Analysis of the impact of different strategies on voltage fluctuations

Rapid changes in loads in the system faults, and shock at the load end can lead to voltage fluctuations. The larger the value of ΔU, the higher the RMS value of the 10 cycles of the voltage. The operating process is analyzed with 4–4.2 s at 10 cycles.

Result in Fig. 14 indicate that voltage variation changes periodically, and the peak voltage fluctuation of the proposed strategy was observed to decrease from 2.92 to 2.86. compared to Harmonics as one of the important factors for voltage fluctuation, and it was noted that improving the harmonic distortion rate improved the voltage fluctuation challenges with respect to time. To reduce the voltage fluctuation better peak and valley regulation was conducted, to balance supply and demand. The results show that the optimization strategy has a good effect on improving power quality such as harmonics and voltage fluctuations.

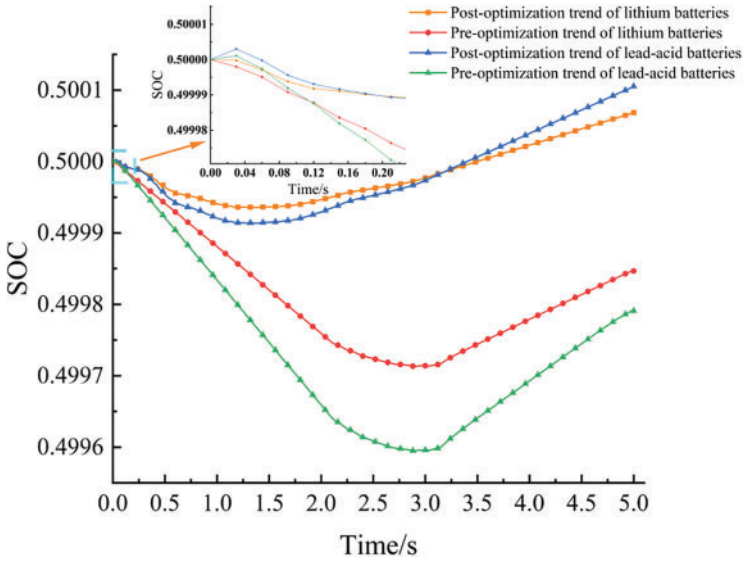

Figure 13: Curves of the trend of SOC for electrochemical energy storage

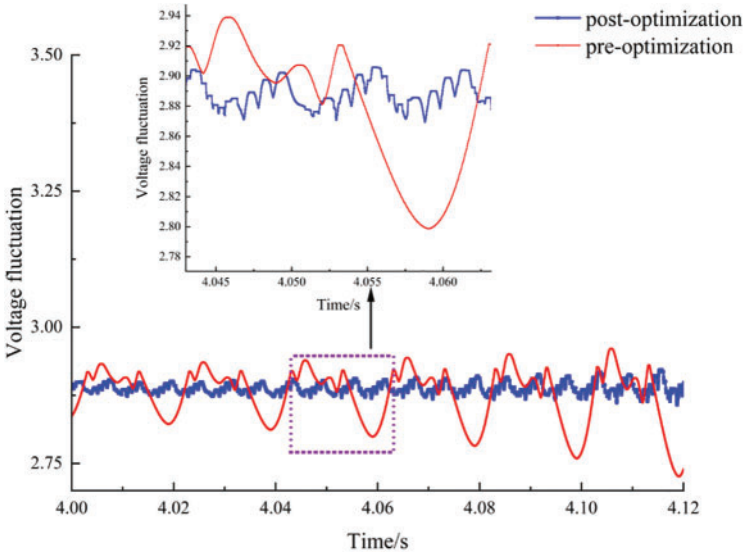

Figure 14: Curves comparing the effect of voltage fluctuation

5 Conclusion

This paper proposes a new operation strategy for wind and solar hybrid energy storage systems. The strategy is optimized by power allocation and a multi-objective genetic algorithm, and the conclusions are drawn following:

(1) It was observed that the proposed strategy performed power decomposition and determined the minimum fluctuation volume limit for initial allocation. The optimized objectives function of dynamic cost with the lowest integrated cost and longer life cycle was depicted and verified to be effective in enhancing wind power fluctuation, economy, and battery cycle life. The power decomposition obtained by the proposed strategy can be widely used in frequency division energy storage technology, which provides a reference for smoothing the fluctuation of wind and wind output while improving the economy.

(2) The results show that the proposed electro-thermal hybrid energy management strategy based on the SOC reduces the depth of discharge and increases the cycle life by 145 times. Likewise, it reduces battery overuse, maintains sufficient capacity to smooth fluctuations, reduces cost, and improves battery cycle life. This management strategy provides a new way to solve the problem of over-charge and over-discharge extremes by providing a feasible stabilizing power system volatility.

(3) In general, the proposed strategy adds an electro-thermal HESS complementary mechanism, which improves thermal energy utilization and reduces the cost of hybrid energy storage, while the complementary mechanism improves the service period of the electrochemical energy system. However, the role of the battery for high-frequency compensation is not enough, and the system combined with power storage such as supercapacitors needs further research to better utilize the advantages of HESS.

Acknowledgement: The authors would like to thank the new energy storage Department of Ordos Energy Research Institute of Peking University for its important support in providing RT-LAB and other simulation tools, and the Key Laboratory of Wind Energy and Solar Energy of Inner Mongolia University of Technology for providing the necessary test site for this paper. Finally, the authors thank the editors and anonymous reviewers for their critical and constructive comments.

Funding Statement: This work was supported by a Horizontal Project on the Development of a Hybrid Energy Storage Simulation Model for Wind Power Based on an RT-LAB Simulation System (PH2023000190); the Inner Mongolia Natural Science Foundation Project and the Optimization of Exergy Efficiency of a Hybrid Energy Storage System with Crossover Control for Wind Power (2023JQ04).

Author Contributions: The authors confirm contribution to the paper as follows: study conception and design: Caifeng Wen, Hongliang Hao; fund preparation: Hongliang Hao, Yuwen Zhang; data collection and sorting: Hao Qiu, Chaoyu Wang; draft manuscript writing: Feifei Xue, Ning Yang; paper translation: Edwin E. Nyakilla. All authors reviewed the results and approved the final version of the manuscript.

Availability of Data and Materials: The authors ensure the authenticity and validity of the materials and data in the article.

Ethics Approval: Not applicable.

Conflicts of Interest: The authors declare no conflicts of interest to report regarding the present study.

References

[1] D. Suchet, A. Jeantet, T. Elghozi, and Z. Jehl, "Defining and quantifying intermittency in the power sector," *Energies*, vol. 13, no. 13, 2020, Art. no. 3366. doi: 10.3390/en13133366.

[2] N. M. Kumar, A. Ghosh, and S. S. Chopra, "Power resilience enhancement of a residential electricity user using photovoltaics and a battery energy storage system under uncertainty conditions," *Energies*, vol. 13, no. 16, 2020, Art. no. 4193. doi: 10.3390/en13164193.

[3] M. Lucu, I. Gandiaga, and H. Camblong, "A critical review on self-adaptive Li-ion batteryageing models," *J. Power Sources*, vol. 401, pp. 85–101, 2018. doi: 10.1016/j.jpowsour.2018.08.064.

[4] A. Ali, G. Abbas, M. Keerio, E. Touti, Z. Ahmed and O. Alsalman, "A bi-level techno-economic optimal reactive power dispatch considering wind and solar power integration," *IEEE Access*, vol. 11, pp. 62700–62819, 2023. doi: 10.1109/ACCESS.2023.3286930.

[5] J. Kabouris and F. D. Kanellos, "Impacts of large-scale wind penetration on designing and operation of electric power systems," *IEEE Trans. Sustain. Energy.*, vol. 1, no. 2, pp. 107–114, 2010. doi: 10.1109/TSTE.2010.2050348.

[6] G. Ren, W. Wang, J. Wan, F. Hong, and K. Yang, "A novel metric for assessing wind and solar power complementarity based on three different fluctuation states and corresponding fluctuation amplitudes," *Energy Convers. Manag.*, vol. 278, no. 7830, 2023, Art. no. 116721. doi: 10.1016/j.enconman.2023.116721.

[7] Q. Hassan, S. Algburi, A. Z. Sameen, H. M. Salman, and M. Jaszczur, "A review of hybrid renewable energy systems: Solar and wind-powered solutions: Challenges, opportunities, and policy implications," *Results Eng.*, vol. 20, no. 18, 2023, Art. no. 101621. doi: 10.1016/j.rineng.2023.101621.

[8] A. Kumar, Y. R. Sood, and R. N. Mahia, "Hybrid energy system simulation and modelling incorporating wind and solar power," in *IEEE Int. Stud. Conf. Elect., Elect. Comput. Sci. (SCEECS)*, Bhopal, India, 2024, pp. 1–5. doi: 10.1109/SCEECS61402.2024.

[9] I. Rahimi, M. R. Nikoo, and A. H. Gandomi, "Techno-economic analysis for using hybrid wind and solar energies in Australia," *Energy Strategy Rev.*, vol. 47, no. 7, 2023, Art. no. 101092. doi: 10.1016/j.esr.2023.101092.

[10] I. J. Fernández, C. F. Calvillo, and J. Boal, "Capacity fade and aging models for electric batteries and optimal charging strategy for electric vehicles," *Energy*, vol. 60, no. 12, pp. 35–43, 2023. doi: 10.1016/j.energy.2013.07.068.

[11] Y. Guo, B. Ming, Q. Huang, Z. Yang, Y. Kong and X. Wang, "Variation-based complementarity assessment between wind and solar resources in China," *Energy Convers. Manag.*, vol. 278, 2023, Art. no. 116726. doi: 10.1016/j.enconman.2023.116726.

[12] M. A. Adesanya *et al.*, "Dynamic modeling and techno-economic assessment of hybrid renewable energy and thermal storage systems for a net-zero energy greenhouse in South Korea," *Clean Technol. Environ. Policy*, vol. 26, no. 13, pp. 551–576, 2024. doi: 10.1007/s10098-023-02656-3.

[13] Y. Gong, Q. Jiang, and R. Baldick, "Ramp event forecast based wind power ramp control with ESS," *IEEE Trans. Power Syst.*, vol. 31, no. 3, pp. 1831–1844, 2016. doi: 10.1109/TPWRS.2015.2445382.

[14] R. Pedruzzi *et al.*, "Review of mapping analysis and complementarity between solar and wind energy sources," *Energy*, vol. 283, no. 15, 2023, Art. no. 129045. doi: 10.1016/j.energy.2023.129045.

[15] T. Okazaki, Y. Shirai, and T. Nakamura, "Concept study of wind power utilizing direct thermal energy conversion and thermal energy storage," *Renew. Energy*, vol. 83, no. 10, pp. 332–338, 2015. doi: 10.1016/j.renene.2015.04.027.

[16] Y. Xiao, C. Zou, M. Dong, H. Chi, Y. Yan and S. Jiang, "Feasibility study: Economic and technical analysis of optimal configuration and operation of a hybrid CSP/PV/wind power cogeneration system with energy storage," *Renew. Energy*, vol. 225, no. 8, 2024, Art. no. 120273. doi: 10.1016/j.renene.2024.120273.

[17] J. Graça Gomes *et al.*, "Hybrid solar PV-wind-battery system bidding optimisation: A case study for the Iberian and Italian liberalised electricity markets," *Energy*, vol. 263, no. 15, 2023, Art. no. 126043. doi: 10.1016/j.energy.2022.126043.

[18] L. Qing, M. Usman, M. Radulescu, and M. Haseeb, "Towards the vision of going green in South Asian region: The role of technological innovations, renewable energy and natural resources in ecological footprint during globalization mode," *Resour. Policy*, vol. 88, no. 11, 2024, Art. no. 104506. doi: 10.1016/j.resourpol.2023.104506.

[19] U. Kahraman and I. Dincer, "Development and assessment of an integrated underground gasification system for cleaner outputs," *Energy*, vol. 285, no. 15, 2023, Art. no. 128676. doi: 10.1016/j.energy.2023.128676.

[20] J. Tian, S. Zhou, and Y. Wang, "Assessing the technical and economic potential of wind and solar energy in China—A provincial-scale analysis," *Environ. Impact Assess. Rev.*, vol. 102, 2023, Art. no. 107161. doi: 10.1016/j.eiar.2023.107161.

[21] A. S. Alghamdi, "Optimal power flow of hybrid wind/solar/thermal energy integrated power systems considering costs and emissions via a novel and efficient search optimization algorithm," *Appl. Sci.*, vol. 13, no. 8, 2023, Art. no. 4670. doi: 10.3390/app13084760.

[22] P. Pérez-López *et al.*, "ENVI-PV: An interactive Web Client for multi-criteria life cycle assessment of photovoltaic systems worldwide," *Photovolt: Res. Appl.*, vol. 25, no. 10, pp. 484–498, 2016. doi: 10.1002/pip.2841.

[23] M. Parhizi, M. Pathak, J. K. Ostanek, and A. Jain, "An iterative analytical model for aging analysis of Liion cells," *J. Power Sources*, vol. 517, no. 1, 2022, Art. no. 230667. doi: 10.1016/j.jpowsour.2021.230667.

[24] J. Yang, H. Chi, M. Cheng, M. Dong, S. Li and H. Yao, "Performance analysis of hydrogen supply using curtailed power from a solar-wind-storage power system," *Renew. Energy*, vol. 212, no. 2, pp. 1005–1019, 2023. doi: 10.1016/j.renene.2023.05.094.

[25] M. S. Alam *et al.*, "Solar and wind energy integrated system frequency control: A critical review on recent developments," *Energies*, vol. 16, no. 2, 2023, Art. no. 812. doi: 10.3390/en16020812.

[26] C. Wen, Q. Wang, Y. Cao, L. Zhang, and W. Wang, "Correlation analysis of wind turbine temperature rise and exergy efficiency based on field-path coupling," *Energy Eng.*, vol. 120, no. 7, pp. 1603–1619, 2023. doi: 10.32604/ee.2023.027074.

[27] C. Wen, B. Zhang, Y. Dai, W. Wang, and W. Xie, "The correlation between the power quality indicators and entropy production characteristics of wind power + energy storage systems," *Energy Eng.*, vol. 121, no. 10, pp. 2961–2979, 2024. doi: 10.32604/ee.2024.041677.

[28] T. Liu, J. Yang, Z. Yang, and Y. Duan, "Techno-economic feasibility of solar power plants considering PV/CSP with electrical/thermal energy storage system," *Energ. Convers. Manag.*, vol. 255, no. 2, 2022, Art. no. 115308. doi: 10.1016/j.enconman.2022.115308.

[29] R. P. Kandi, M. M. Sudharmini, A. Suryan, and S. Nižetić, "State of the art and future prospects for TEG-PCM Systems: A review," *Energy Sustain. Dev.*, vol. 74, no. 6, pp. 328–348, 2023. doi: 10.1016/j.esd.2023.04.012.

[30] M. Emamjome Kashan, A. S. Fung, and A. Hossein Eisapour, "Insulated concrete form foundation wall as solar thermal energy storage for cold-climate building heating system," *Energy Convers. Manag. X*, vol. 19, no. 9, 2023, Art. no. 100391. doi: 10.1016/j.ecmx.2023.100391.

[31] B. Koçak, A. I. Fernandez, and H. Paksoy, "Review on sensible thermal energy storage for industrial solar applications and sustainability aspects," *Solar Energ.*, vol. 209, no. 8, pp. 135–169, 2020. doi: 10.1016/j.solener.2020.08.081.

[32] S. Guo, Q. Liu, J. Sun, and H. Jin, "A review on the utilization of hybrid renewable energy," *Renew. Sustain. Energ. Rev.*, vol. 91, pp. 1121–1147, 2018. doi: 10.1016/j.rser.2018.04.105.

[33] L. Liu and Z. Wang, "The development and application practice of wind-solar energy hybrid generation systems in China," *Renew. Sustain. Energ. Rev.*, vol. 13, no. 6–7, pp. 1504–1512, 2009. doi: 10.1016/j.rser.2008.09.021.

[34] M. K. Deshmukh and S. S. Deshmukh, "Modeling of hybrid renewable energy systems," *Renew. Sustain. Energ. Rev.*, vol. 12, no. 1, pp. 235–249, 2008. doi: 10.1016/j.rser.2006.07.011.

[35] S. Rekik and S. El Alimi, "Optimal wind-solar site selection using a GIS-AHP based approach: A case of Tunisia," *Energy Convers. Manag. X*, vol. 18, no. 2, 2023, Art. no. 100355. doi: 10.1016/j.ecmx.2023.100355.

[36] B. Ghobadian, G. Najafi, H. Rahimi, and T. F. Yusaf, "Future of renewable energies in Iran," *Renew. Sustain. Energ. Rev.*, vol. 13, no. 3, pp. 689–695, 2009. doi: 10.1016/j.rser.2007.11.010.

[37] H. X. Yang, L. Lu, and J. Burnett, "Weather data and probability analysis of hybrid photovoltaic-wind power generation systems in Hong Kong," *Renew. Energ.*, vol. 28, no. 11, pp. 1813–1824, 2003. doi: 10.1016/S0960-1481(03)00015-6.

[38] H. J. Wagner, "Introduction to wind energy systems," in *EPJ Web of Conf.*, Bochum, Germany, 2020, vol. 246. doi: 10.1051/epjconf/202024600004.

[39] H. J. Wagner, "Introduction to wind energy systems," in *EPJ Web of Conf.*, Bochum, Germany, 2018, vol. 189. doi: 10.1051/epjconf/201818900005.

[40] J. Fan, X. Huang, J. Shi, K. Li, J. Cai and X. Zhang, "Complementary potential of wind-solar-hydro power in Chinese provinces: Based on a high temporal resolution multi-objective optimization model," *Renew. Sustain. Energ. Rev.*, vol. 184, 2023, Art. no. 113566. doi: 10.1016/j.rser.2023.113566.

[41] L. Yao, Y. Wang, and X. Xiao, "Concentrated solar power plant modeling for power system studies," *IEEE Trans. Power Syst.*, vol. 12, no. 2, pp. 1–12, 2023. doi: 10.1109/TPWRS.2023.3301996.

[42] L. Liu *et al.*, "Climate change impacts on planned supply-demand match in global wind and solar energy systems," *Nat. Energy*, vol. 8, no. 8, pp. 870–880, 2023. doi: 10.1038/s41560-023-01304-w.

[43] M. L. Sørensen, P. Nystrup, M. B. Bjerregård, J. K. Møller, P. Bacher and H. Madsen, "Recent developments in multivariate wind and solar power forecasting," *Wires Energ. Environ.*, vol. 12, no. 2, 2022, Art. no. 465. doi: 10.1002/wene.465.

[44] J. Nematian and I. Rahimi, "Feasibility study of using renewable energies in Iranian Seas: A comparative study," *Renew. Energy*, vol. 189, no. 7, pp. 383–391, 2022. doi: 10.1016/j.renene.2022.02.109.

[45] R. Hemmati, S. M. S. Ghiasi, and A. Entezariharsini, "Power fluctuation smoothing and loss reduction in grid integrated with thermal-wind-solar-storage units," *Energy*, vol. 152, no. 2, pp. 759–769, 2018. doi: 10.1016/j.energy.2018.04.004.

[46] H. Su, S. Song, and X. Wang, "Probabilistic calculation of tidal currents for wind powered systems using PSO improved LHS," *Energy Eng.*, vol. 121, no. 11, pp. 3289–3303, 2024. doi: 10.32604/ee.2024.054643.

[47] S. K. Sarker, S. R. Fahim, N. Sarker, K. Z. Tayef, A. B. Siddique and D. Datta, "Ancillary voltage control design for adaptive tracking performance of microgrid coupled with industrial loads," *IEEE Access*, vol. 9, pp. 143690–143706, 2021. doi: 10.1109/ACCESS.2021.3121548.

[48] A. Mahesh and K. S. Sandhu, "A genetic algorithm based improved optimal sizing strategy for solar-wind-battery hybrid system using energy filter algorithm," *Front. Energy*, vol. 14, no. 1, pp. 139–151, 2017. doi: 10.1007/s11708-017-0484-4.

[49] X. Ma, M. Deveci, J. Yan, and Y. Liu, "Optimal capacity configuration of wind-photovoltaic-storage hybrid system: A study based on multi-objective optimization and sparrow search algorithm," *J. Energy Storage*, vol. 85, 2024, Art. no. 110983. doi: 10.1016/j.est.2024.110983.

[50] M. Gao, Z. Han, C. Zhang, P. Li, D. Wu and P. Li, "Optimal configuration for regional integrated energy systems with multi-element hybrid energy storage," *Energy*, vol. 277, 2023, Art. no. 127672. doi: 10.1016/j.energy.2023.127672.